Science and Technology for Energy Transition **78**, 6 (2023)

https://doi.org/10.2516/stet/2023002

Available online at:
stet-review.org

REGULAR ARTICLE OPEN ACCESS

Fatigue analysis of brazing structures with fin-plate-side bar in Liquefied Natural Gas (LNG) heat exchangers under cryogenic conditions

Hongqiang Ma[1,2,*], Jiwei Jia[1,2,3], Yu Liu[1], Xinmei Luo[1], Caiqin Hou[2], and Gang Wang[2]

[1] School of Civil Engineering and Architecture, East China Jiaotong University, Nanchang 330013, PR China
[2] School of Civil Engineering, Lanzhou University of Technology, Lanzhou 730050, PR China
[3] Faculty of Environment and Life, Beijing University of Technology, Beijing 100124, PR China

Received: 15 November 2022 / Accepted: 6 February 2023

Abstract. The purpose of this study is to evaluate the fatigue life of heat exchangers used for Liquefied Natural Gas (LNG) and to ensure its structural safety, the alternating stress of brazing structures under cryogenic conditions was analyzed with a Finite Element Model (FEM). Stress concentrations occurred at the brazed joint with a maximum alternating stress amplitude of 153.45 MPa. The fatigue life of brazed structures during the continuous cool-down and heat-up conditions was evaluated based on the ASME standard and the maximum alternating stress amplitude. Meanwhile, structure parameters have been analyzed for their influence on fatigue life. There are four main structure factors to influence the life cycle: the brazing seam, the fin thickness, the fin distance, and the fin height. The life cycle will decrease with increasing the fin distance, fin height, and brazing seam thickness, and it will increase with increasing the fin thickness. In addition, in order to predict fatigue life, a calculating model has been established based on the main factors. Finally, the fatigue life of brazing structures was also tested by experiment, and the microstructure was also analyzed for the fatigue fracture surface. It is clear that brittle fractures along the brazing seam and ductile fractures at the fin roots should be the primary failure modes. The study provides a base for LNG aluminum heat exchanger design, manufacture, and safe operation.

Keywords: Brazing structure, Fatigue assessment, Structure parameter, Predict model, Fracture mechanism.

Nomenclature

LNG	Liquefied Natural Gas
NG	Natural Gas
MR	Mixed Refrigerant

Symbols

a	Coefficient
b	Coefficient
C	Coefficient of S-N curve
k	Coefficient of S-N curve
K_f	Fatigue strength reduction factor
K_e	Fatigue penalty factor
K_v	Poisson rate correction factor
m	Material constant used for the fatigue knock-down factor
n	Material constant used for the fatigue knock-down factor
N	Fatigue life
S	Stress amplitude, MPa
S_y	Material yield strength at the mean temperature, MPa
S_{alt}	Equivalent alternating stress amplitude, MPa
S_{PS}	Allowable limit value in the range of primary plus secondary equivalent stress, MPa
X	Raw data
$X_{\min}$	The minimum value in raw data
$X_{\max}$	The maximum value in raw data
X_{norm}	The data after normalization processing
f	Fin thickness, mm
g	Fin distance, mm
T_{MR}	MR temperature, K
P_{NG}	NG pressure, MPa
δ	Brazing seam thickness, mm
h	Fin height, mm

* Corresponding author: mahq2014@sina.com

ΔT	Difference between NG temperature and MR temperature, K
$Y_{\text{life-cycles}}$	Fatigue life of brazing structure
σ_{eq}	von-Mises equivalent stress, MPa
$\sigma_{\text{eq}}^{\text{th}}$	Equivalent thermal stress, MPa
$\sigma_{\text{eq}}^{\text{str}}$	Equivalent structure stress, MPa
${}^{m}\sigma_{ij}$	Stress tensor at the evaluation location when located in the valley point moments, MPa
${}^{n}\sigma_{ij}$	Stress tensor at the evaluation location when located in the peak point moments, MPa
${}^{m}\sigma_{ij}^{\text{th}}$	Stress tensor due to local thermal stress in the location and time point at the valley point, MPa
${}^{n}\sigma_{ij}^{\text{th}}$	Stress tensor due to local thermal stress in the location and time point at the peak point, MPa
v_p	Modified Poisson ratio
v_e	Elastic Poisson ratio
$\Delta\sigma_{ij}^{\text{th}}$	Range of stress tensor due to local thermal stress at the evaluation location, MPa
$\Delta\sigma_{\text{ij}}$	Range of stress tensor at the evaluation location, MPa
ΔS_{str}	Equivalent structural stress range of each load cycle, MPa
ΔS_p	Range of primary plus secondary plus peak equivalent stress, MPa
ΔS_{th}	Local equivalent thermal stress, MPa
ΔS_n	Range of primary plus secondary equivalent stress, MPa

1 Introduction

As a critical piece of equipment in the cryogenic treatment process of natural gas liquefaction [1, 2], aluminum plate-fin heat exchangers have been widely used because of their compact structure [3, 4], moderate pressure drop [5], light weight [6], large heat transfer area [7], excellent heat transfer efficiency [8, 9], simultaneous multiple media heat transfer [10, 11] and other advantages. Usually, the heat exchanger will be accompanied by frequent cool-down and heat-up during the daily operation. During this process, the heat exchanger will expand and contract rapidly as its temperature and pressure change. And inside the heat exchanger, the thermal stress cycles will eventually generate [12, 13]. This will induce to generate alternating stress, and fatigue failure will have occurred in the heat exchanger.

Currently, experiments [14] and finite element methods [15] have primarily been used to study the fatigue failure of heat exchangers. These studies were primarily concerned with heat exchanger fatigue failure at high temperatures and pressures [16, 17]. For example, the steady-state method was used to investigate heat exchanger fatigue failure under high-pressure conditions [18]. At the joint location of tube-tube sheets, the maximum equivalent thermal stress has occurred, the temperature gradient at this location is higher than in other regions, and the life cycles are shortest. At the same time, some experiments and microstructure analyses were also done to evaluate the failure behavior of heat exchangers in [19, 20]. It can be obtained that the main failure model is the creep and fatigue under high temperature-pressure conditions. Additionally, a comparison is also made between the failure models at the same design parameter [21]. It can be seen that creep failure should be emphasized in high temperature conditions because the influence of creep is greater than that of fatigue. Moreover, the influence of material properties [22], geometry [23, 24], and operation parameters [25] was also investigated for the structural strength of heat exchangers. The main factors have been obtained to impact that. In summary, the heat exchanger damage caused by creep and fatigue under high temperature and pressure is the main focus of the above investigations. The fatigue damage of heat exchangers is mainly ductile thermal fatigue failure under high temperature-pressure conditions. Under the cryogenic condition, the influence of creep can be completely negligible for heat exchanger failure. And the failure model will mainly belong to the cryogenic brittle [26] or ductile–brittle thermal fatigue damage [27] at this condition.

Meanwhile, several scholars have also studied plate-fin heat exchanger failure behavior under cryogenic conditions [28, 29]. For example, the strength of heat exchangers has been analyzed in the different operation processes in our previous works [30, 31], and the optimum operation method has also been proposed to ensure heat exchanger safety operation. In addition, there has also been considered the effect of the structure and operation characteristics of plate-fin heat exchangers when investigating their strength [32, 33]. And some key elements are discovered that have an impact on its safe operation. However, the fatigue failure of heat exchangers has not been deeply investigated under cryogenic circumstances. The aluminum brazing structure with fin-plate-side bar (also called the brazing structure) of plate-fin heat exchangers is easily broken. If the structure parameters are unreasonably selected in the designing and manufacturing process, it will accelerate the fatigue failure of heat exchangers. Consequently, it is necessary that the fatigue failure of brazing structures at the different structure parameters will be further investigated under the cryogenic thermal-structural cyclic stress condition.

In this paper, an analysis of the alternating stress within cryogenic brazing structures will be carried out through the use of a Finite Element Model (FEM). Then, the continuous cool-down and heat-up conditions will be used to calculate the alternating stress. Based on the ASME standard, the fatigue life of brazing structures will be evaluated according to the maximum alternating stress amplitude. Meanwhile, the impact of structural characteristics on fatigue life of it will also be studied for brazing structures. In addition, it will be established a fatigue life calculation model, and the fatigue life of brazing structures will be evaluated in accordance with this model. Finally, the fatigue life of brazing structures will also be tested by a fatigue experiment, and the microstructure will be analyzed for the fatigue fracture surface of that.

2 Finite Element Analysis (FEA)

2.1 FEA model

Figure 1 is the diagram of brazing structures. The brazing structure is mainly composed of plate, fin and side bar. They will be stacked and staggered in terms of the design requirements and finally brazed in a vacuum brazing furnace. According to refs. [32, 33], the impact of layer and channel numbers on the results will not be considered in the simulation. So an analysis of brazing structure fatigue life will be carried out using a finite element model. In this model, the channel and fin layer numbers are 9 and 4, respectively. Meanwhile, in order to evaluate the fatigue life of brazing structures, a small distance in the z-direction will be used since the heat exchanger will have a relatively small temperature gradient along its length. In addition, a semi-symmetric structure will be applied in this model due to the repeatability and symmetry of brazing structures. The semi-symmetric model of brazing structure is shown in Figure 2. Table 1 is the structure characteristics parameters of brazing structures.

2.2 Boundary condition

Due to the effect of pressure and temperature fields during actual operation, the brazing structure will experience thermal-structural stress. In this paper, the coupling approach of thermal and structure will be used to assess how thermal stress and structure stress are distributed in brazing structures. The boundary conditions are shown as follows.

To represent the convective heat transfer process between NG/MR and the wall of brazing structures, the convective heat transfer boundary will be loaded on the surface between NG/MR and the brazing structure. Similarly, in order to express the effect of MR pressure or NG pressure on the surface of brazing structures, the pressure boundary will also be loaded on the surface between NG/MR and the brazing structure.

Additionally, due to the symmetry of brazing structures, the adiabatic and symmetry boundary will also be used on the right wall of that. At the same time, in order to express the free sliding of brazing structures along the horizontal direction of support structures, there will be a fixed boundary imposed on the bottom surface in the y-direction. The external load action will not be considered in this paper. The contacts between plate and fin will be implemented by the Bonded from ANSYS software. Figure 3 is the diagram of the boundary conditions.

2.3 Physical properties of AL3003/AL4004

In this paper, the side bar, the fins and plates, and the brazing seam will be made of AL3003 and AL4004, respectively. The elastic-plastic theory will be used to analyze the fatigue of brazing structures. The temperature has a stronger impact on the elastic modulus and thermal expansion coefficient of AL3003/AL4004 according to the literature [32, 33]. Therefore, the effect of temperature will be considered for that Table 2 is the physical properties of AL3003/AL4004.

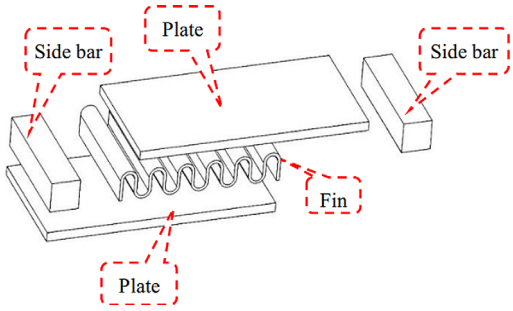

Figure 1. The diagram of brazing structures.

2.4 Mesh verification

In this section, the model shown in Figure 2 will be discretized by the structured grid, and the grid will be intensified in sensitive regions, such as the brazed joint. Compared with other areas, the brazed joint will have denser nodes, as shown in Figure 4. It is necessary to study the impact of grid node numbers on the calculation results at the h_{MR} = 1000 W/(m^2 K), h_{NG} = 1500 W/(m^2 K), P_{MR} = 0.4 MPa, P_{NG} = 7.1 MPa, T_{MR} = 150 K and T_{NG} = 155 K to ensure simulation accuracy and save time. At the same time, four grid groups of 152,530, 198,450, 247,965 and 272,380 nodes are chosen to study the stress conditions of brazing structures, respectively. Figure 5 shows the relationship between stress and the total number of nodes. It can be found that the stress approximately remains constant when the total number of nodes is changed from 247,965 to 272,380. Therefore, we will use a brazing structure consisting of 272,380 grid nodes to study its fatigue life in this work.

3 Fatigue analysis

3.1 Fatigue cycle

The fatigue life study of brazing structures in this paper will take into account the influence of pressure and temperature load for it. The convective boundary and the NG/MR pressure, respectively, will be used to define the thermal and pressure load.

The alternating stress in the brazing structure is very small during normal operation according to the literature. However, the alternating stress during the cool-down and heat-up operation is relatively higher compared with normal operation [34]. Therefore, the fatigue failure of brazed structures is analyzed under the continuous cool-down and heat-up cycles in this paper. At the same time, the brazed structure will generate cyclic alternating stress due to frequent cool-down and heat-up during the daily operation. This will eventually induce the fatigue failure of brazed structures [35]. The cyclic alternating stress will appear a maximum and minimum peak values in the fatigue cycle

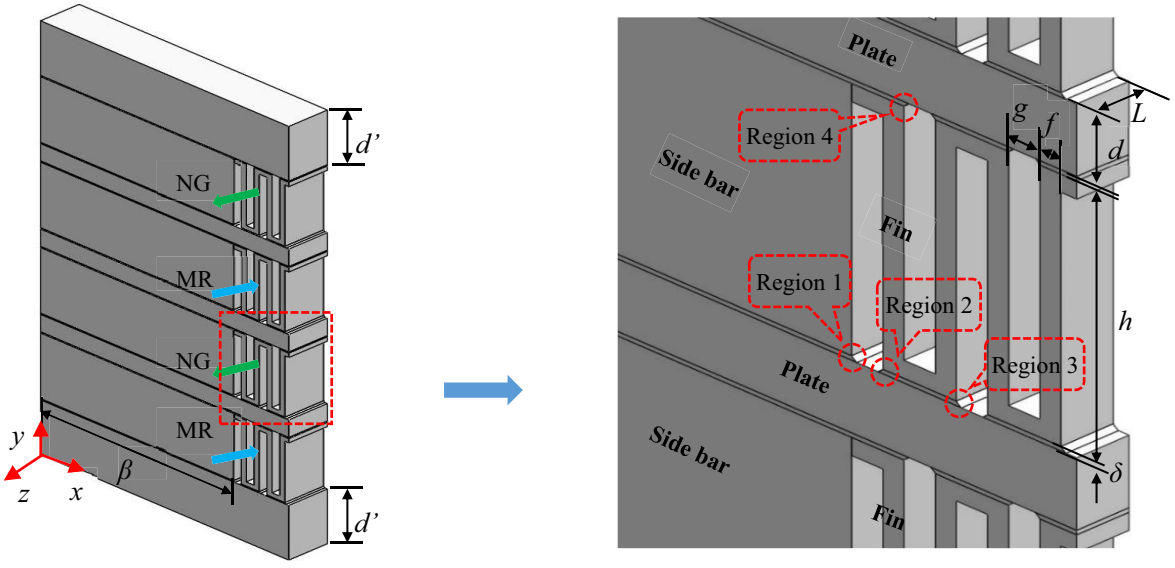

Figure 2. The semi-symmetric model of brazing structures.

Table 1. The structure characteristic parameter of brazing structures (along the y-direction).

Layer	Fin thickness f/mm	Fin distance g/mm	Cover plate thickness d/mm	Brazing seam thickness δ/mm	Effective length L/mm	Plate thickness d/mm	Side bar length β/mm	Fin height h/mm
1	0.4	0.6	5.0	0.1	1.0	1.6	25.0	6.0
2	0.4	0.6	5.0	0.1	1.0	1.6	25.0	6.0
3	0.4	0.6	5.0	0.1	1.0	1.6	25.0	6.0
4	0.4	0.6	5.0	0.1	1.0	1.6	25.0	6.0

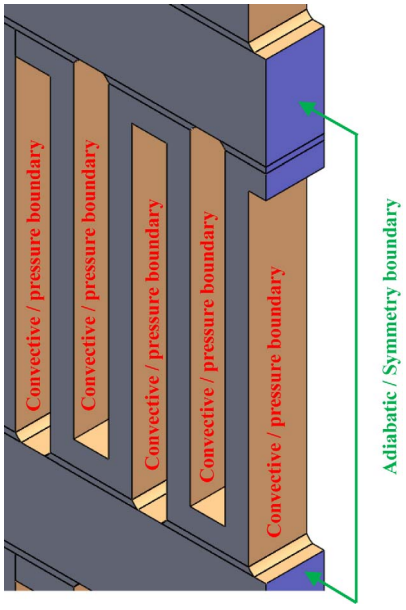

Figure 3. The diagram of boundary condition.

process, which are defined as peak and valley points. According to the calculation results, the peak and valley point will appear at the following two conditions from Table 3. Figure 6 shows the variation of NG or MR temperature and pressure during the cool-down and heat-up cycle. Meanwhile, the cycle load spectrum is also determined in terms of the peak and valley point of brazed structures in the frequent cool-down and heat-up cycle [36].

3.2 Fatigue Assessment Method

In this paper, the ASME standard will be used to evaluate the fatigue life of brazing structures [37]. In the calculation method of alternating stress amplitude, some factors have been considered in this standard, including the weld type and material, heat exchanger surface finish, local notch or effect of the weld and so on. Thus, the following equation can be used to express the alternating stress amplitude in accordance with the ASME standard:

$$S_{\text{alt}} = \frac{K_f \cdot K_e \cdot \Delta S_{\text{str}} + K_v \cdot \Delta S_{\text{th}}}{2}. \quad (1)$$

Table 2. The physical properties of AL3003/AL4004.

Material	Temperature/K	Elasticity modulus/ GPa	Expansion coefficient $(10^{-6})/1/K$	Yield strength/ MPa	Poisson ratio	Specific heat J/(kg K)	Density kg/m^3	Conductivity W/(m K)
AL3003	145	74.5	14.4	145	0.33	962	2740	159
	175	73.2	15.9					
	195	72.4	16.9					
	250	70.6	19.7					
	305	68.9	22.4					
AL4004	145	99.6	14.5	142	0.35	864	2710	155
	175	98.8	14.6					
	195	98.2	14.7					
	250	96.4	14.9					
	305	94.6	15.1					

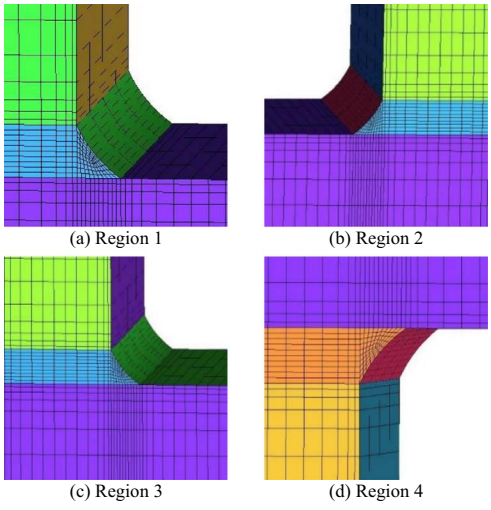

Figure 4. Local mesh.

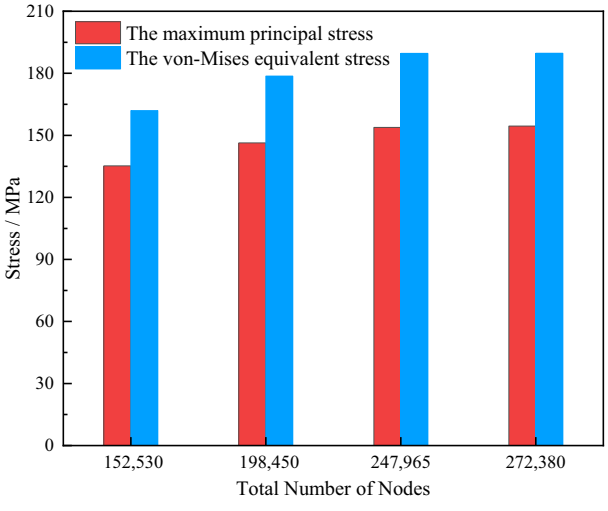

Figure 5. The relationship between stress and the total number of nodes.

Table 3. The peak and valley condition.

Location	Type	Temperature (K)	Pressure (MPa)
Valley point	NG	298	0
	MR	298	0
Peak point	NG	155	7.1
	MR	150	0.4

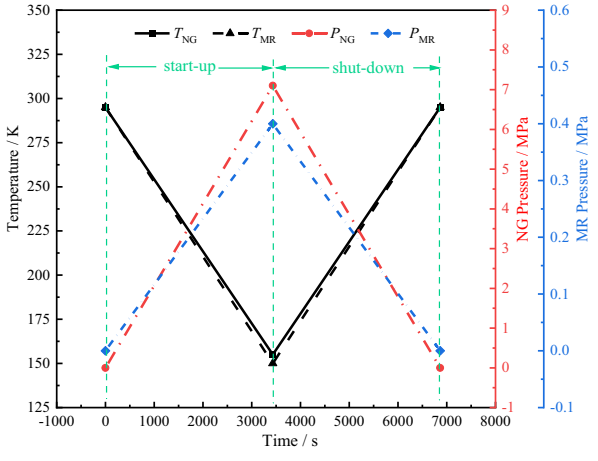

Figure 6. The variation of temperature and pressure.

According to the equation above, S_{alt} will be mainly calculated by ΔS_{str} and ΔS_{th}. K_f, K_e and K_v will be used to further revise the calculation results. In this work, based on von Mises stress criterion, the thermal and structural stress of brazing structure will be analyzed during continuous cool-down and heat-up cycles by ANSYS software, and then the equivalent thermal and structural stress are obtained. Calculation of the equivalent structure stress range and equivalent local thermal stress range for each load cycle will be carried out based on the following equation:

$$\Delta S_{\mathrm{str}} = (\Delta S_p - \Delta S_{\mathrm{th}}) = \frac{1}{\sqrt{2}} \left[\begin{array}{c} 0.5 \sum\limits_{i=1,j=1,i\neq j}^{i=3,j=3} \left(\Delta\sigma_{ii} - \Delta\sigma_{jj}\right)^2 \\ +3 \sum\limits_{i=1,j=1,i\neq j}^{i=3,j=3} \Delta\sigma_{ij}^2 \end{array} \right], \tag{2}$$

$$\Delta S_{\mathrm{th}} = \frac{1}{\sqrt{2}} \left[0.5 \sum_{i=1,j=1,i\neq j}^{i=3,j=3} \left(\Delta\sigma_{ii}^{\mathrm{th}} - \Delta\sigma_{jj}^{\mathrm{th}}\right)^2 \right]^{0.5}. \tag{3}$$

According to equations (2) and (3), the equivalent structure and equivalent local thermal stress range of each load cycle will be related to the stress tensor range. They can be written as:

$$\Delta\sigma_{ij} = \left({}^{m}\sigma_{ij} - {}^{m}\sigma_{ij}^{\mathrm{th}}\right) - \left({}^{n}\sigma_{ij} - {}^{n}\sigma_{ij}^{\mathrm{th}}\right), \tag{4}$$

$$\Delta\sigma_{ij}^{\mathrm{th}} = {}^{m}\sigma_{ij}^{\mathrm{th}} - {}^{n}\sigma_{ij}^{\mathrm{th}}. \tag{5}$$

In equation (1), the value of K_f is 2.5 [37]. Meanwhile, the progressive deformation behavior due to alternating stress will be modified by the K_e [38, 39], it can be obtained by the following equations [37]:

$$K_e = \begin{cases} 1.0, & \Delta S_n \leq S_{\mathrm{PS}} \\ 1.0 + \dfrac{(1-n)}{n(m-1)}\left(\dfrac{\Delta S_n}{S_{\mathrm{PS}}} - 1\right), & S_{\mathrm{PS}} \leq \Delta S_n \leq mS_{\mathrm{PS}} \\ \dfrac{1}{n}, & \Delta S_n \geq mS_{\mathrm{PS}} \end{cases}. \tag{6}$$

The material constants m and n are dependent on the hardening process and material characteristics, are used for the fatigue knock-down factor in the simplified elastic-plastic analysis. The results of finite element analysis in this work show that the equivalent stress amplitude of the sum of primary and secondary equivalent stress would be less than the allowed limit (175 MPa). So the K_e will be assumed to be 1.0 according to equation (6). Therefore, $m$and $n$will not be considered in this paper. Additionally, the value of K_v in equation (1) will be calculated by the following equation [37]. In this paper, the value of K_v is about 0.3 [40, 41].

$$K_v = \left(\frac{1-v_e}{1-v_p}\right), \tag{7}$$

$$v_p = \max\left[0.5 - 0.2\left(\frac{S_y}{S_{\mathrm{alt}}}\right), v_e\right]. \tag{8}$$

After obtaining the equivalent structure and thermal stress by the FEA method in Section 2, the amplitude of equivalent alternating stress can be obtained by substituting that into equation (1). Then, the life cycles can be calculated in terms of the comparison between the equivalent alternating stress and the *S-N* curve. In fact, the fatigue life is mainly related to the equivalent alternating stress and material properties. During the process of cool-down and heat-up cycles, the equivalent alternating stress will be eventually generated in the brazing structures due to the combined action of structure and thermal tress induced by temperature and pressure, respectively. And the uniaxial fatigue test is only a way to generate the equivalent alternating stress inside material. So it should be feasible to apply the uniaxial *N-S* curve to analyze the fatigue life when the material is isotropic. In this paper, the uniaxial *S-N* curve obtained by the group test method, which the survival probability is about 95% will be used to calculate the life cycles [42]. The expression of the *S-N* curve is as follows:

$$S^k \cdot N = C. \tag{9}$$

The logarithm is taken on both sides of the above equation.

$$\lg S = a + b \lg N, \tag{10}$$

among

$$\begin{cases} a = \lg C/k \\ b = -1/k \end{cases}. \tag{11}$$

The values of a and b will be determined using the least-squares method, which are 3.0564 and −0.25373, respectively.

4 Result and discussion

4.1 Fatigue assessment

The brazed joint is the weakest part of brazing structures, which makes this area prone to fatigue failure. The brazed joint regions (as shown in Fig. 2) will be selected to analyze the alternating stress and to evaluate the fatigue failure of brazing structures in this work.

Figures 7 and 8 show the distribution of equivalent alternating stress amplitude at the brazed joint and maximum shear stresses. Compared to the other location, the brazed joint has higher maximum shear stress and equivalent alternating stress amplitudes. They will reach a peak of 79.14 MPa and 153.45 MPa, respectively. The gradient is very large at the brazed joint. This is because the material properties between the base metal and brazing seam are incompletely matched, and the thermal expansion and cold contraction are incompletely synchronized and constrained to a certain extent. The stress transfer inside the brazing structure will be blocked at the brazed joint. So a higher stress gradient will be induced at the brazed joint and the surrounding area. The high amplitude of equivalent alternating stress will eventually be generated at this location with the stress concentrations gradually accumulating. And the fatigue failure will most likely occur at this location. According to the ASME standard, the fatigue life at the brazing joint will be calculated and the life cycle is about 3311.

4.2 The influence of structure parameters

This section will analyze the relationship between the life cycles of brazing structures and structure parameters based

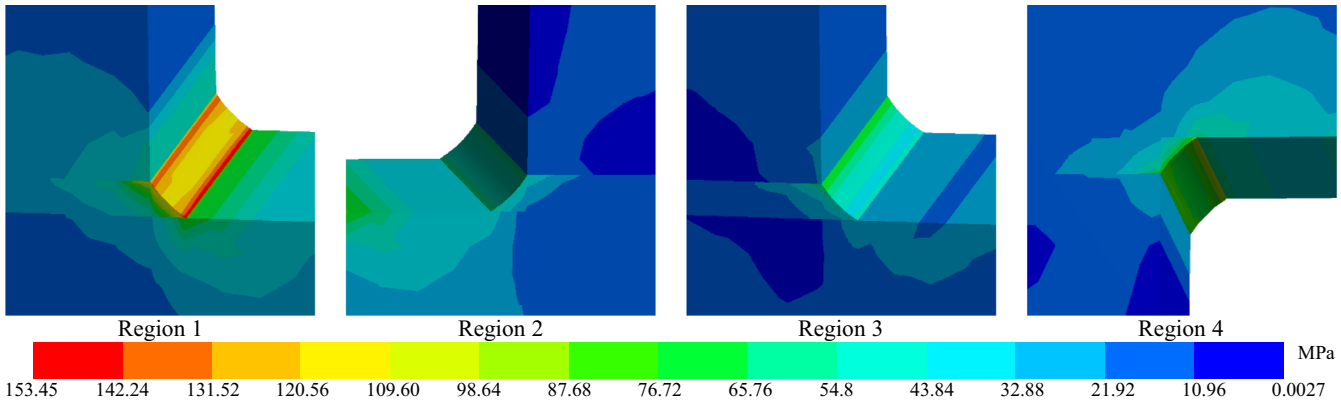

Figure 7. The distribution of equivalent alternating stress amplitude at the brazed joint of brazing structures.

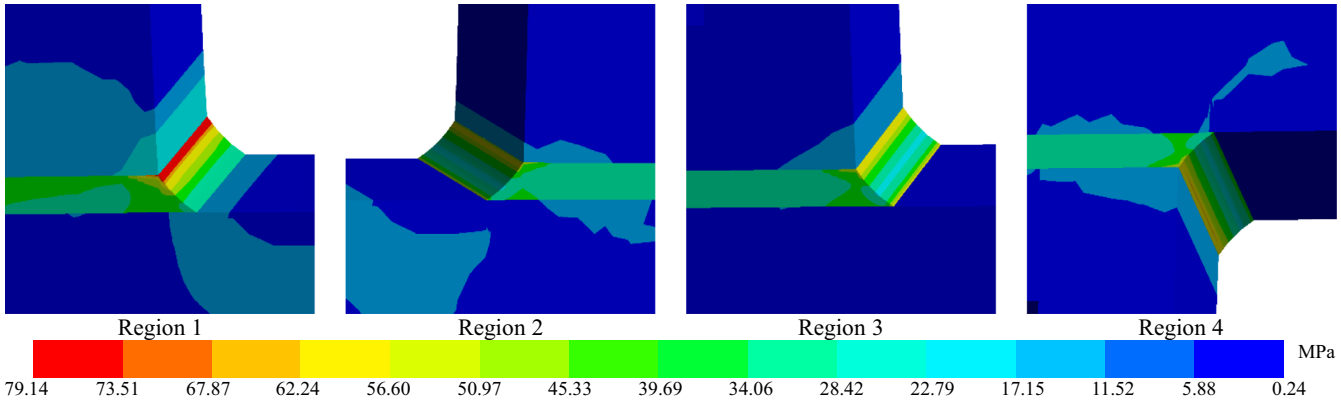

Figure 8. The distribution of maximum shear stress at the brazed joint of brazing structures.

on the ASME standard and equivalent alternating stress amplitude calculated by the FEM, and further investigate the impact law of structure parameters on fatigue life.

4.2.1 The brazing seam thickness

The relationship between life cycles and brazing seam thickness at various plate thicknesses is shown in Figure 9. The results demonstrate that life cycles have an approximately parabolic relationship with brazing seam thickness and will gradually decrease with brazing seam thickness increase. In other words, the larger brazing seam thickness is, the smaller life cycle is. At the same time, it can also be found from Figure 9 that the plate thickness will have a slight impact on life cycles. In order to further investigate how brazing seam thickness impacts fatigue life, Figure 10 also shows the relationship between stresses and brazing seam thickness at various plate thicknesses. It is clear that as the brazing seam thickness gradually increases, so will the thermal and structural stress. At the same time, the plate thickness will have a slight effect on the stress. In actuality, the temperature gradient at the brazed joint will be the main cause to induce the thermal stresses at this location. Increasing the brazing seam thickness will change the temperature distribution and further increase the temperature gradient at the brazed joint. This will be the main reason thermal stresses gradually increase with the brazing seam thickness. Meanwhile, the decrease of life cycles with the brazing seam thickness will be collectively induced by the thermal and structural stresses. And the brazing seam thickness should be a sensitive factor to impact the fatigue life of brazing structures.

4.2.2 The fin height

The relationship between life cycles and fin height at various side bar lengths is shown in Figure 11. The results show that the life cycles are approximately linear and gradually decrease with the increase of fin height, while the side bar length has little impact on it. Meanwhile, the relationship between stresses and fin height is also given in Figure 12. It can be found that the structure stress will gradually increase with the fin height while the thermal stress will approximately constant with that. Meanwhile, the stress will also be slightly influenced by the side bar length. In other words, the structure stress will be the main reason to induce the decrease of life cycles with the fin height, which is also a sensitive factor to effect the fatigue life. Compared with Figure 9, the life cycles will linearly decrease with the fin height while nonlinearly decrease

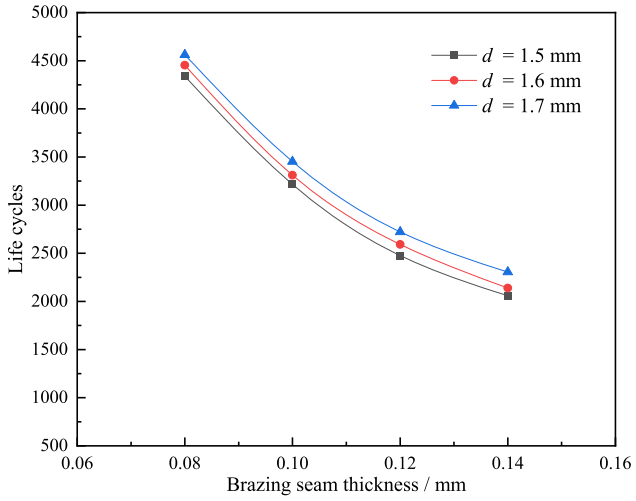

Figure 9. The life cycles *vs.* brazing seam thickness.

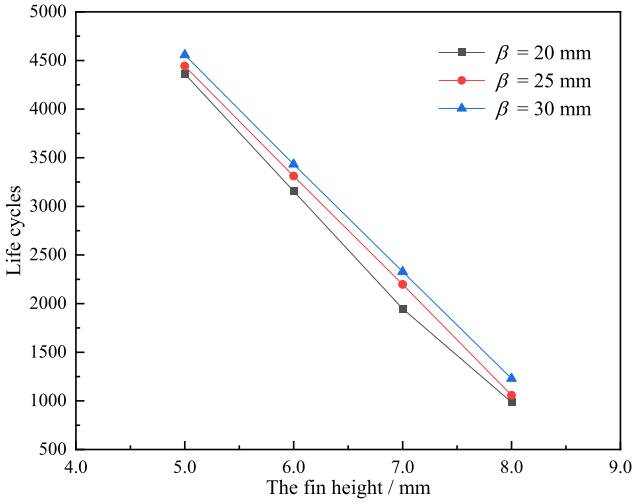

Figure 11. The life cycles *vs.* fin height.

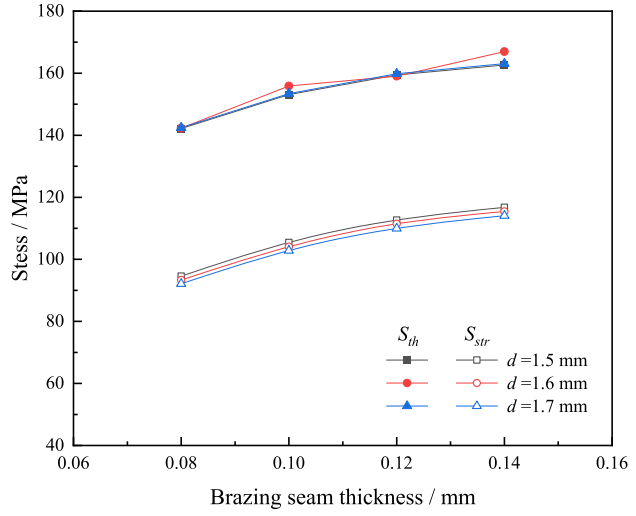

Figure 10. The stresses *vs.* brazing seam thickness.

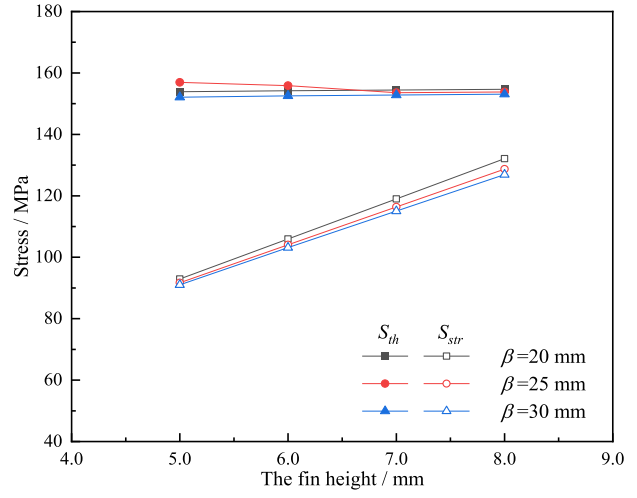

Figure 12. The stresses *vs.* fin height.

with brazing seam thickness. This may be because the thermal stresses will obviously increase with the brazing seam thickness at the brazed joint due to the change of temperature gradient, and the fin height has a slight impact on it.

4.2.3 The fin distance

The relationship between life cycles and fin distance at various brazing seam thicknesses is shown in Figure 13. It is clear that when fin distance increase, life cycles will linearly decrease. Meanwhile, the brazing seam thickness also has an obvious impact on fatigue life. It is consistent with the conclusion in Figure 7. Although the fin distance has an obvious impact on life cycles, it will also have a small effect on that compared with Figures 9 and 11. The relationship between stresses and fin distance at various brazing seam thicknesses is shown in Figure 14. It can be seen that the structure stress will gradually increase with the fin distance, while the thermal stress will decrease firstly and then approximately remain constant with that. Through the contrast between structural and thermal stress, it can be found that the thermal stress will be slightly changed with the fin distance while the change of structural stress will be obvious with the fin distance. In other words, the decrease of life cycles with the fin distance will be mainly induced by the structural stresses.

4.2.4 The fin thickness

The relationship between life cycles and fin thickness at various fin heights is shown in Figure 15. It is clear that the life cycles will gradually increase with the fin thickness, and is approximately a parabolic relationship with that. It can also be found that the life cycles also are largely impacted by fin height. The results will be similar to that from Figure 11. Meanwhile, the relationship between stresses and fin thickness at various fin heights will also be given

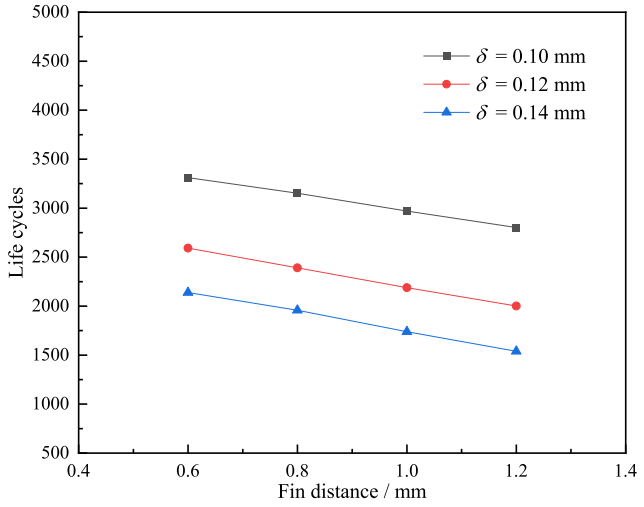

Figure 13. The life cycles *vs.* fin distance.

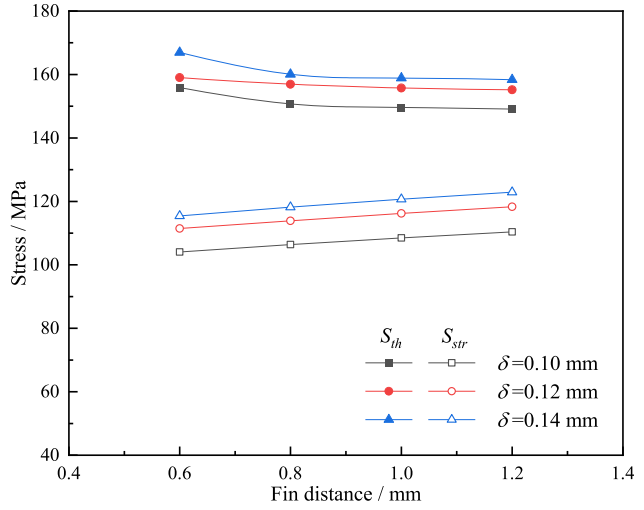

Figure 14. The stresses *vs.* fin distance.

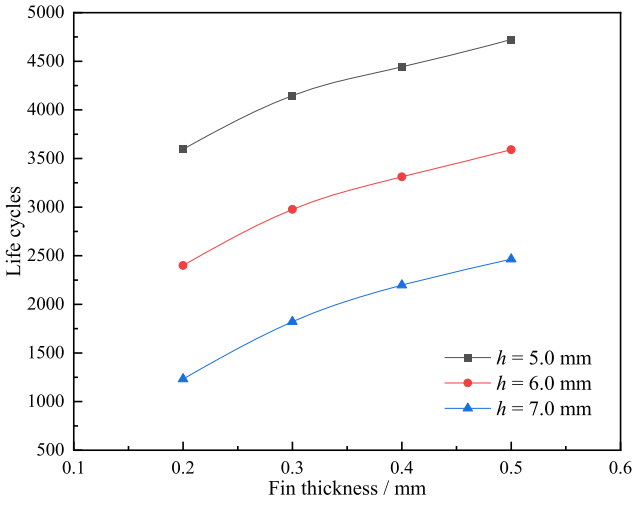

Figure 15. The life cycles *vs.* fin thickness.

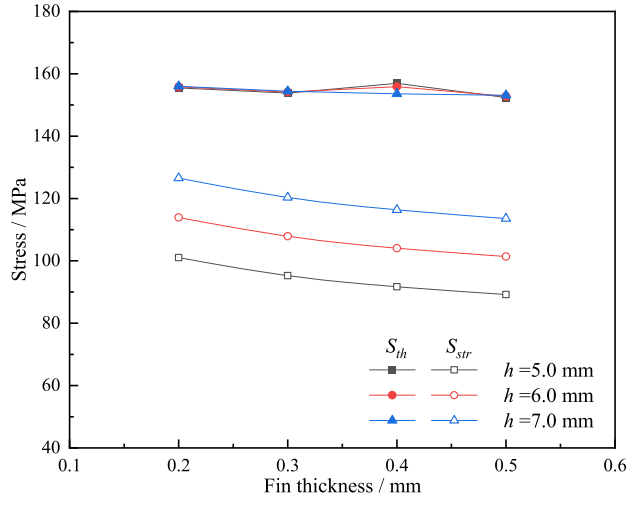

Figure 16. The stresses *vs.* fin thickness.

in Figure 16. The findings demonstrate that as fin thickness increases, structural stress gradually decreases while thermal stress is only slightly impacted. In addition, the fin height also has a larger influence on structure stress. This will be consistent with the conclusion in Figure 12. Therefore, increasing the fin thickness will decrease the structural stress. This will further prolong the fatigue life of heat exchangers.

4.3 Sensitivity analysis

The sensitivity between life cycles and structure parameters will be analyzed in more detail in order to further study how the structure parameters impact fatigue life. In this section, the structure parameters will be normalized according to the following equation:

$$X_{\text{norm}} = \frac{X - X_{\min}}{X_{\max} - X_{\min}}. \tag{12}$$

In equation (12), X is the raw data, X_{norm} is the data after normalization, $X_{\min}$ is the minimum value in raw data, and $X_{\max}$ is the maximum value in raw data.

Figure 17 shows the relation between life cycles and the data after normalization for the structure parameters. The results show that the life cycles will linearly decrease with fin height and fin distance while nonlinearity decrease with brazing seam thickness. And it will also nonlinearity increase with fin thickness, and linearly increase with the plate thickness and side bar length. According to the datum from Figure 17, the life cycles will decrease by 76.18%, 22.80% and 51.96% with the fin height, fin distance and brazing seam thickness, respectively. It will increase by 49.63%, 7.37% and 8.78% with the fin thickness, plate thickness and side bar length, respectively. Obviously, the life cycles will be slightly impacted by plate thickness and side bar length. The main structural factors that influence fatigue life are the brazing seam thickness, fin height, fin distance and fin thickness.

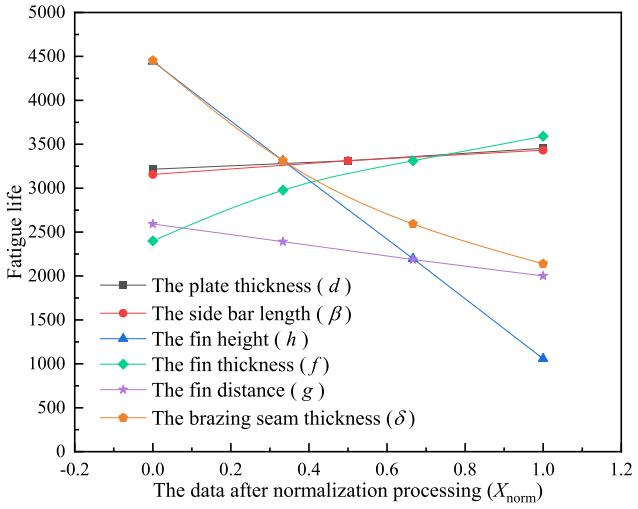

Figure 17. The relation between life cycles and the data after normalization.

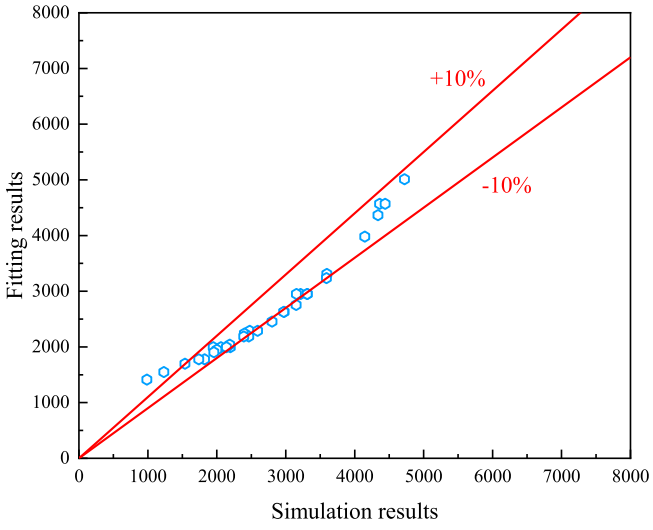

Figure 18. The error between simulation result and prediction result.

4.4 Fatigue life prediction model

According to equations (1) and (10), we can find that the thermal stress and structural stress will determine the equivalent alternating stress, and they will further affect fatigue life. In addition, according to Section 4.2, the main structural parameters that will affect the structural stress are the brazing seam thickness, fin height, fin distance, and fin thickness. And the brazing seam thickness will also be the main structure parameter to affect the thermal stress. In order to more easily and conveniently obtain thermal stress and structural stress in practical engineering, and further predict the life cycles of brazing structures, the relationship between thermal stress and structural stress and structure parameters will be fitted based on considering the above influence factors according to the datum of Section 4.2. The fitting results of that are as follows, respectively:

$$S_{\mathrm{str}} = -3644.93\delta^2 + 1166.66\delta + 12.89h + 10.21g - 13.00\ln(f) - 70.88, \tag{13}$$

$$S_{\mathrm{th}} = -4825\delta^2 + 1400.20\delta + 61.11. \tag{14}$$

Then, the relationship between the equivalent alternating stress and each effect factor can be obtained by combining equations (12) and (13) into (1), as follows:

$$S_{\mathrm{alt}} = -5279.91\delta^2 + 1668.36\delta + 16.11h + 12.76g - 16.25\ln(f) - 79.43. \tag{15}$$

Finally, the fatigue life predict model will be established by combining equations (15) and (10), and it can be expressed by the following:

$$\lg N = 12.0 - 3.9\lg\left[-5279.91\delta^2 + 1668.36\delta + 16.11h + 12.76g - 16.25\ln(f) - 79.43\right]. \tag{16}$$

Figure 18 is the error between the simulation result and the prediction result from equation (16). The result shows that the error will be almost within 10% for $\delta = 0.08 - 0.14$ mm, $f = 0.2 - 0.5$ mm, $h = 5.0 - 7.0$ mm, $g = 0.6 - 1.2$ mm, $P_{\mathrm{NG}} = 7.1$ MPa, $P_{\mathrm{MR}} = 0.4$ MPa, $T_{\mathrm{MR}} = 150$ K and $T_{\mathrm{NG}} = 155$ K. Therefore, the prediction and simulation results will be approximately consistent, and this prediction model can be applied to actual engineering.

4.5 Experiment test analysis

The fatigue life of brazing structures will be tested in order to further study the fatigue fracture mechanism of that by the fatigue test machine with the *MTS Landmark* 370.10 when the maximum cyclic load is 5.51 KN, maximum cyclic stress amplitude is 61.25 MPa, and loading frequency is about 40 Hz. According to the results in Figure 17, the life cycles will be slightly impacted by the side bar length. So the side bar length will be ignored in the test specimen of brazing structure, which will be shown in Figure 19. Figure 20 is the diagram of the fatigue test process. Meanwhile, the microstructure on the fatigue fracture surface will also be observed by the Scanned Electron Microscope (SEM) of Japan Hitachi SU8010.

Figure 21 is the macroscopic morphology on the fatigue fracture surface. It can be seen that the fatigue fracture surface is uneven and very rough. The fatigue fracture will be mainly occurred along the brazing seam, and the fracture of some local areas will also be generated at the fin root. This may be mainly induced by the mismatch of material properties between the base metal and brazing seam. The stress concentration will be occurred along the brazing seam during the loading process, and the fatigue crack will be gradually generated at the brazed joint. Under the action of cyclic stress, the fatigue cracks will gradually expand along the brazing seam. This is consistent with the conclusion from Figures 7 and 8. Meanwhile, the life cycles from the experiment will also be compared with that from the

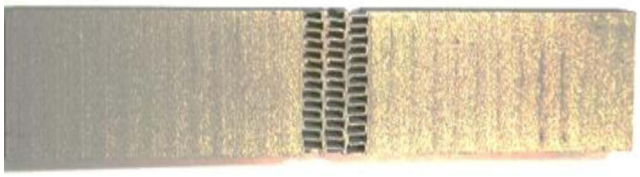

Figure 19. The test specimen of brazing structures.

Figure 20. The diagram of the fatigue test process.

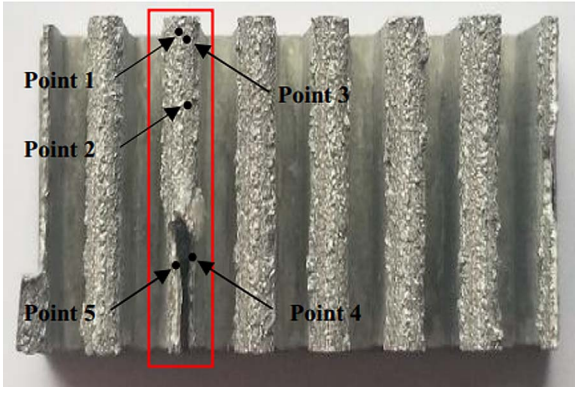

Figure 21. The macroscopic morphology on the fatigue fracture surface.

finite element analysis based on Sections 2 and 3. The results are about 5728 and 5239 from the experiment and the finite element analysis, respectively. This will further verify that the finite element analysis is reliable in this paper.

The local microstructures of brazing structures in points 1–5 in the red line from Figure 21 will be further analyzed in order to study the fatigue mechanism of that. Figure 22 is the microstructure at point 1. On the fracture surface, the typical river pattern cleavage fracture will be observed, and the orientation of the fracture is shown in the figure. The metal is polycrystalline and the orientation is disordered. The cleavage cracks will not be expanded along a single crystallographic plane while along many parallel cleavage planes in the crystal grains. In the forward

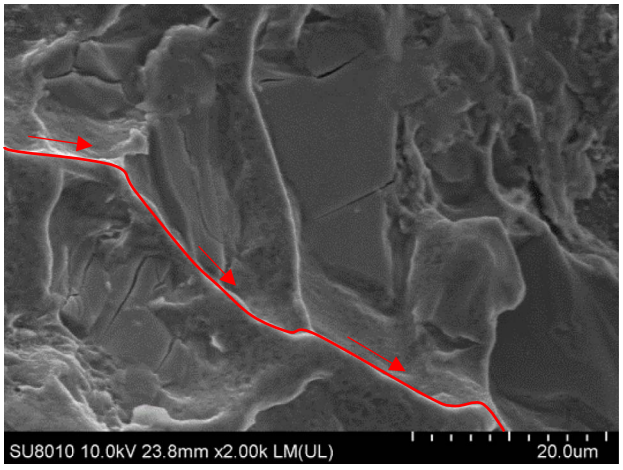

Figure 22. The microstructure at point 1.

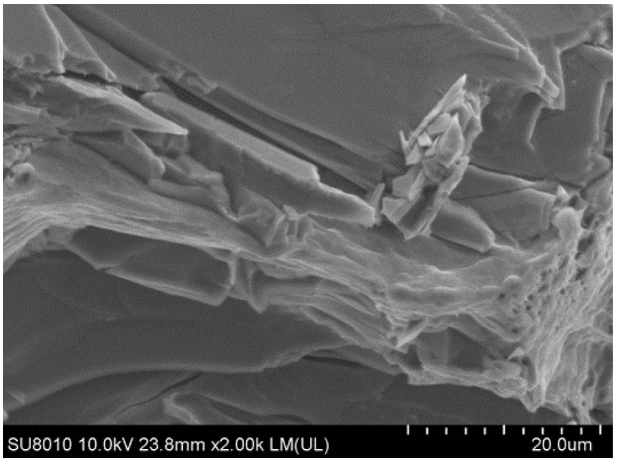

Figure 23. The microstructure at point 2.

expansion process of cleavage cracks on the different cleavage planes, cleavage cracks will be connected by secondary cleavage, screw dislocation intersection, and tearing or matrix-twin interface cracking. This will induce a crack pattern similar to the river, so it is called the river pattern. For the river pattern, the small rivers will tend to merge into large rivers in order to reduce the energy consumption of cleavage crack expansion. Therefore, the expansion direction of local fatigue cracks on the fracture surface can be shown in Figure 22.

Figure 23 is the microstructure at point 2. It can be seen that many flat areas can be observed on the fracture surface, these are called cleavage steps. This is mainly formed by secondary cleavage of cleavage cracks on the different cleavage planes. The cleavage step is a typical sign to prove the cleavage fracture. At the same time, some cleavage steps also can be observed in Figure 22. Many cleavage steps in Figures 22 and 23 indicate that brittle fracture is the main fracture mechanism along the brazing seam because that cleavage fracture is a typical characteristic of brittle fracture. In addition, Figure 24 is the microstructure at point 3. On the fracture surface, secondary

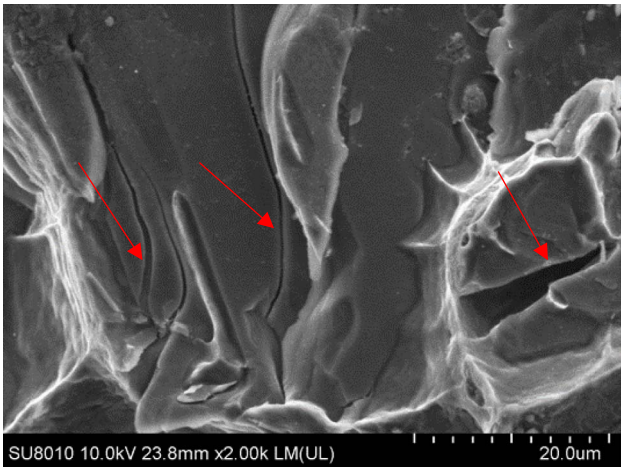

Figure 24. The microstructure at point 3.

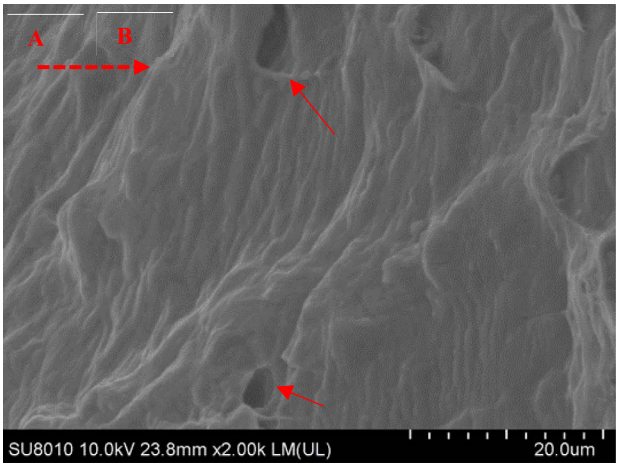

Figure 25. The microstructure at point 4.

cracks can be seen in Figure 24. This may be induced by the energy concentration at the crack front in the experiment, or the cracks encounter second phase in the expansion process.

Figure 25 is the microstructure at point 4. On the fracture surface, it is possible to notice a series of basic parallel striations, and they are typical mechanical fatigue striations. This is mainly caused by the slip between crystals in the loading process. The fatigue striation often will be thought a typical characteristic of fatigue under the electron microscope, and it is an important basis to prove the fatigue failure of the specimen. Generally, the direction of fatigue striation is vertical with the expansion direction of the local fatigue cracks, and it is convex outward along the expansion direction of that. Therefore, the expansion direction of local fatigue crack on the fracture surface is from A to B, as shown in Figure 25. In addition, Figure 26 is the microstructure at point 5. According to Figures 25 and 26, the findings demonstrate that there are some dimple morphology on the fracture surface because the internal crystals of specimens are subjected to tensile

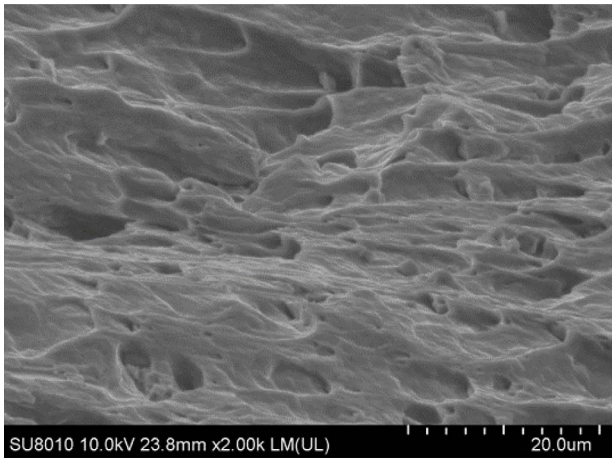

Figure 26. The microstructure at point 5.

normal stress or shear stress in the loading process. This will further indicate that ductile fracture is the main fracture mechanism at the fin root.

5 Conclusion

A Finite Element Model (FEM) was built in this paper to obtain the alternating stress of brazing structures under cryogenic circumstances. Then, calculated maximum alternating stress amplitude and the ASME standard was combined to evaluate the fatigue life of brazing structures. The impact of structure parameters on life cycles was also further investigated. A prediction model was proposed to estimate the life cycles of brazing structures. Finally, the fatigue life of brazing structures was also tested, and the microstructure was analyzed on the fatigue fracture surface. The followings are main conclusions of this paper by above study:

1. The maximum alternating stress amplitude may occur at the brazed joint, so the brazing joint will be the most likely position to occur the fatigue failure, and the life cycle is the shortest at this position and about 3311.
2. There will have four main structural parameters to impact the life cycle of brazing structures, they are the fin height, the fin distance, the brazing seam, and the fin thickness, respectively. Life cycles will have a negative correlation with the fin distance, fin height, and brazing seam thickness, and a positive correlation with the fin thickness.
3. A prediction model is proposed to evaluate the life cycles of brazing structures based on the simulation datum. The critical structure parameters will be considered to affect the fatigue life of brazing structures in this prediction model. The error between prediction and simulation results will be within 10%.
4. The fatigue fracture of brazing structures will be mainly generated along the brazing seam and at the fin root of some local areas. The brittle fracture and

ductile fracture will be the main fatigue fracture model along the brazing seam and at the fin root, respectively.

Acknowledgments. In this note, the author expresses his gratitude to the National Natural Science Foundation of China (51808275), the Postdoctoral Science Foundation of China (2018M643768), and the Natural Science Foundation of Gansu Province (1606RJZA059) for providing funding support for the project.

References

1 Zheng W.K., Wang Y.S., Cui Q.J., Yang Z.Y., Cai W.H., Chen J., Jiang Y.Q. (2018) Sloshing effect on gas-liquid distribution performance at entrance of a plate-fin heat exchanger, *Exp. Therm. Fluid Sci.* **93**, 419–430.
2 Li J.R., Hu H.T., Xie Y., Chen Y.D. (2021) Two-phase flow boiling characteristics in plate-fin channels at offshore conditions, *Appl. Therm. Eng.* **187**, 116595.
3 Zheng W.K., Jiang Y.Q., Cai W.H. (2019) Distribution characteristics of gas-liquid mixture in plate-fin heat exchangers under sloshing conditions, *Exp. Therm. Fluid Sci.* **101**, 115–127.
4 Martins G.S.M., Santiago R.S., Beckedorff L.E., Possamai T. S., Oba R., Oliveira J.L.G., Oliveira A.A.M., Paiva K.V. (2022) Structural analysis of gasketed plate heat exchangers, *Int. J. Press. Vessel. Pip.* **197**, 104634.
5 Cheng X., Yao Y.P., Wu H.Y. (2021) An experimental investigation of flow boiling characteristics in silicon-based groove-wall microchannels with different structural parameters, *Int. J. Heat Mass Transf.* **168**, 120843.
6 Li W., Lin Y.H., Zhou K., Li J.Y., Zhu J. (2019) Local heat transfer of saturated flow boiling in vertical narrow microchannel, *Int. J. Therm. Sci.* **145**, 105996.
7 Li Y.F., Xia G.D., Ma D.D., Yang J.L., Li W. (2019) Experimental investigation of flow boiling characteristics in microchannel with triangular cavities and rectangular fins, *Int. J. Heat Mass Transf.* **148**, 119036.
8 Zheng W.K., Jiang Y.Q., Cai W.H., Li F.Z., Wang Y.S. (2021) Numerical investigation on the distribution characteristics of gas-liquid flow at the entrance of LNG plate-fin heat exchangers, *Cryogenics* **113**, 103227.
9 Li Y., Li Y.X., Hu Q.H., Wang W.C., Xie B., Yu X.C. (2015) Sloshing resistance and gas-liquid distribution performance in the entrance of LNG plate-fin heat exchangers, *Appl. Therm. Eng.* **82**, 182–193.
10 Vaisi A., Javaherdeh K., Moosavi R. (2022) Experimental investigation of the thermal performance in a single-component two-phase flow in multistream multi-fluid plate-fin heat exchangers, *Int. J. Therm. Sci.* **171**, 107194.
11 Zhu J.L., Zhang W., Li Y.X., Ji P., Wang W.C. (2019) Experimental study of flow distribution in plate-fin heat exchanger and its influence on natural gas liquefaction performance, *Appl. Therm. Eng.* **155**, 398–417.
12 Jiang W.C., Gong J.M., Tu S.T. (2017) Fatigue life prediction of a stainless steel plate-fin structure using equivalent-homogeneous-solid method, *Mater. Des.* **32**, 10, 4936–4942.
13 Ge L., Jiang W.C., Wang Y., Tu S.T. (2018) Creep-fatigue strength design of plate-fin heat exchanger by a homogeneous method, *Int. J. Mech. Sci.* **146–147**, 221–233.
14 Yang X.J., Liu M.H., Liu Z.Y., Du C.W., Li X.G. (2020) Failure analysis of a 304 stainless steel heat exchanger in liquid sulfur recovery units, *Eng. Fail. Anal.* **116**, 104729.
15 Ando M., Hasebe S., Kobayashi S., Kasahara N., Toyoshi A., Ohmae T., Enuma Y. (2014) Thermal transient test and strength evaluation of a tubesheet structure made of Mod. 9Cr-1Mo steel. Part II: creep-fatigue strength evaluation, *Nucl. Eng. Des.* **275**, 422–432.
16 Romanovski V., Hedberg Y.S., Paspelau A., Frantskevich V., Noël J.J., Romanovskaia E. (2021) Corrosion failure of titanium tubes of a heat exchanger for the heating of dissolving lye, *Eng. Fail. Anal.* **129**, 105722.
17 Liu X.F., Zhu H.Y., Yu C.Y., Jin H.Z., Wang C., Ou G.F. (2021) Analysis on the corrosion failure of U-tube heat exchanger in hydrogenation unit, *Eng. Fail. Anal.* **125**, 105448.
18 Pérez-lvarez R., González-Gómez P., Acosta-Iborra A., Santana D. (2021) Thermal stress and fatigue damage of central receiver tubes during their preheating, *Appl. Therm. Eng.* **195**, 117115.
19 Ali M., Ul-Hamid A., Alhems L.M., Saeed A. (2020) Review of common failures in heat exchangers – Part I: mechanical and elevated temperature failures, *Eng. Fail. Anal.* **109**, 104396.
20 Liu L., Ding N., Shi J.B., Xu N., Guo W.M., Wu C.L.M. (2016) Failure analysis of tube-to-tubesheet welded joints in a shell-tube heat exchanger, *Case Stud. Eng. Fail. Anal.* **7**, 32–40.
21 Chen Y.X., Zhang Y.P., Wang D., Hu S., Huang X.H. (2021) Effects of design parameters on fatigue-creep damage of tubular supercritical carbon dioxide power tower receivers, *Renew. Energy* **176**, 520–532.
22 Jiang W.C., Gong J.M., Tu S.T., Fan Q.S. (2009) A comparison of brazed residual stress in plate-fin structure made of different stainless steel, *Mater. Des.* **30**, 23–27.
23 Jiang W.C., Gong J.M., Tu S.T., Chen H. (2008) Effect of geometric conditions on residual stress of brazed stainless steel plate-fin structure, *Nucl. Eng. Des.* **238**, 1497–1502.
24 Jiang W.C., Gong J.M., Chen H., Tu S.T. (2008) The effect of filler metal thickness on residual stress and creep for stainless-steel plate-fin structure, *Int. J. Press. Vessel. Pip.* **85**, 569–574.
25 Gong J.M., Jiang W.C., Fan Q.S., Chen H., Tu S.T. (2009) Finite element modelling of brazed residual stress and its influence factor analysis for stainless steel plate-fin structure, *J. Mater. Process. Technol.* **209**, 1635–1643.
26 Salem G.B., Chapuliot S., Blouin A., Bompard P., Jacquemoud C. (2018) Brittle fracture analysis of dissimilar metal welds between low-alloy steel and stainless steel at low temperatures, *Procedia Struct. Integr.* **13**, 619–624.
27 An Q., An R., Wang C.Q., Wang H. (2021) Ductile-to-brittle transition in fracture behaviors of common solder alloys over a temperature range down to −150 °C, *Mater. Today Commun.* **29**, 102962.
28 Haider P., Freko P., Lochner S., Reiter S., Rehfeldt S., Klein H. (2019) Design of a test rig for the simulation of startup procedures in main heat exchangers of air separation plants, *Chem. Eng. Res. Des.* **147**, 90–97.
29 Ma H.Q., Jia J.W., Ding R.X., Luo X.M., Peng D.G., Hou C. Q., Wang G., Zhang Y.J. (2022) Numerical investigation on fatigue life of aluminum brazing structure with fin-plate-side bar under the low temperature thermal-structure cyclic stress, *Eng. Fail. Anal.* **131**, 105918.

30 Ma H.Q., Cai W.H., Zheng W.K., Chen J., Yao Y., Jiang Y.Q. (2014) Stress characteristics of plate-fin structures in the cool-down process of LNG heat exchanger, *J. Nat. Gas Sci. Eng.* **21**, 1113–1126.
31 Ma H.Q., Cai W.H., Yao Y., Jiang Y.Q. (2016) Investigation on stress characteristics of plate-fin structures in the heat-up process of LNG heat exchanger, *J. Nat. Gas Sci. Eng.* **30**, 256–267.
32 Ma H.Q., Chen J., Cai W.H., Shen C., Yao Y., Jiang Y.Q. (2015) The influence of operation parameters on stress of plate-fin structures in LNG heat exchanger, *J. Nat. Gas Sci. Eng.* **26**, 216–228.
33 Ma H.Q., Hou C.Q., Yang R.X., Li C.E., Ma B.S., Ren J.Q., Liu Y.M. (2016) The influence of structure parameters on stress of plate-fin structures in LNG heat exchanger, *J. Nat. Gas Sci. Eng.* **34**, 85–99.
34 Zeng Q.P., Li Y.J., Shi J.X., Zhang G.L., Duan Y.D., Zhang Z.H., Su X.D. (2020) Fatigue life analysis of supercharged boiler based on the design by analysis method, *Int. J. Press. Vessel. Pip.* **188**, 104217.
35 González-Gómez P., Gómez-Hernández J., Briongos J.V., Santana D. (2019) Lifetime analysis of the steam generator of a solar tower plant, *Appl. Therm. Eng.* **159**, 113805.
36 Douellou C., Balandraud X., Duc E. (2022) Fatigue characterization by heat source reconstruction under continuously varying stress amplitude, *Int. J. Fatigue* **159**, 106782.
37 ASME Boiler and Pressure Vessel Code (2019) *Section VIII, division 2, alternative rules, rules for construction of pressure vessels, design by analysis approach*.
38 Martins G.S.M., Silva R.P.P.D., Beckedorff L., Monteiro A. S., Paiva K.V., Oliveira J.L.G. (2020) Fatigue performance evaluation of plate and shell heat exchangers, *Int. J. Press. Vessel. Pip.* **188**, 104237.
39 Rondon A., Guzey S. (2017) Fatigue evaluation of the API specification 12F shop welded flat bottom tanks, *Int. J. Press. Vessel. Pip* **149**, 14–23.
40 Hoseinzadeh S., Heyns P.S. (2020) Thermo-structural fatigue and lifetime analysis of a heat exchanger as a feedwater heater in power plant, *Eng. Fail. Anal.* **113**, 104548.
41 Patil R., Anand S. (2017) Thermo-structural fatigue analysis of shell and tube type heat exchanger, *Int. J. Press. Vessel. Pip.* **155**, 35–42.
42 Hobbacher A.F. (2003) *Recommendations for fatigue design of welded joints and components*, International Institute of Welding, IW/IIS3.